JOURNAL OF SOLID STATE CHEMISTRY 75, 355–363 (1988)

On the MnP ⇌ NiAs-Type Transition in $Mn_{0.63}Cr_{0.37}As$: Structural and Thermodynamic Properties

HELMER FJELLVÅG, FREDRIK GRØNVOLD, ARNE KJEKSHUS, AND SVEIN STØLEN

Department of Chemistry, University of Oslo, Blindern, N-0315 Oslo 3, Norway

Received December 16, 1987; in revised form February 19, 1988

The displacive MnP ⇌ NiAs-type structural transition and the coupled magnetic spin conversion in $Mn_{0.63}Cr_{0.37}As$ have been studied by adiabatic shield type calorimetry and by powder X-ray and neutron diffraction. The structural changes, in positional parameters as well as in unit cell dimensions, have been determined for increasing distortion of the NiAs-type structure at temperatures below the transition temperature T_D = 680 K. The observed heat capacity is resolved into contributions from different physical sources. The importance of the dilational contribution, which arises from anharmonicity of the lattice vibrations and from coupled magneto-structural effects, is substantiated. Thermodynamic functions have been evaluated and the values of C_p, $S^\circ_m(T) - S^\circ_m(0)$ and $-\{G^\circ_m(T) - H^\circ_m(0)\}/T$ at 820 K are 59.07, 131.35, and 80.884 J K^{-1} $mole^{-1}$, respectively.

Introduction

In a series of recent papers the magnetic "low" to "high" spin conversion in $MnAs_{1-x}P_x$ has been studied (*1–3*). The conversion, which appears at temperatures below the structural MnP ⇌ NiAs-type transition, gives rise to a peculiar temperature dependence of the magnetic susceptibility and of the heat capacity. The susceptibility anomaly is in principle explained on the basis of the spin fluctuation theory by Katoh and Motizuki (*4*), whereas the heat capacity effect has recently been treated phenomenologically by the present authors (*2*). In the latter treatment the spin conversion is shown to be closely coupled to the structural transition, and the heat capacity effect is macroscopically explained by taking the exceptionally large variation in the thermal expansivity and isothermal compressibility into account. Although similar anomalies in the magnetic susceptibility have been observed in most transition metal substituted MnAs phases, the heat capacity effect has until now only been reported for $MnAs_{1-x}P_x$. The anomalous magnetic susceptibility behavior connected with the spin conversion is clearly seen in $Mn_{1-t}Cr_tAs$, where the conversion, however, extends over a wider temperature range (*5–7*). In spite of this, only weak indications of the "low" to "high" spin conversion are observed in the heat capacity (*8–9*). The spin conversion in $MnAs_{1-x}P_x$ is coupled to the large changes in the crystal structure which occur in the temperature range between T_N and T_D.

0022-4596/88 $3.00

where T_N denotes the magnetic order–disorder temperature and T_D the MnP $\rightleftharpoons$ NiAs-type structural transition temperature. The temperature range between T_N and T_D is considerably wider for $Mn_{0.63}Cr_{0.37}As$ than for $MnAs_{0.88}P_{0.12}$ (*3*) and the thermal expansion coefficient and the isothermal compressibility may be expected to show less pronounced maxima. Still, an appreciable heat capacity contribution from the spin conversion ought to be present.

The present study reports on the magneto-structural MnP $\rightleftharpoons$ NiAs-type transition. The heat capacity of $Mn_{0.63}Cr_{0.37}As$ from 300 to 820 K is determined by adiabatic shield type calorimetry, whereas the crystallographic properties are evaluated from powder X-ray and powder neutron diffraction experiments. The recorded structural data give the temperature dependence of the unit cell parameters and the positional parameters at temperatures between T_N and T_D. These results are compared with earlier findings for related phases, and are also used for resolution of the observed heat capacity. In the evaluation of the higher temperature thermodynamic properties of $Mn_{0.63}Cr_{0.37}As$, the present heat capacity results are combined with the earlier low temperature data (*9*).

Experimental

CrAs and MnAs were synthesized from high-purity Mn flakes (99.99%), Cr flakes (99.999%), and As lumps (99.9999%) from Koch-Light Laboratories Ltd., England. The binary compounds were prepared by heating stoichiometric quantities of the elements in evacuated sealed silica-glass tubes. The temperature in the horizontally positioned furnaces was slowly increased in steps of 30 K per 8 hr to 1173 K for MnAs and 1273 K for CrAs. After cooling to room temperature during one day the samples were crushed and subjected to one further annealing at 1173 K for one week, followed by cooling to room temperature during one day. The $Mn_{0.63}Cr_{0.37}As$ samples were then made from the binary compounds. After a first heat treatment at 1223 K for one week, the ternary samples were crushed, mixed, and reheated for a joint annealing at 993 K for 3 weeks, and finally slowly cooled to room temperature during one day. The characterization of the samples was done by powder X-ray diffraction (Guinier camera, Cu$K\alpha_1$-radiation), and the refined unit cell dimensions [a = 566.1(1), b = 357.6 (1), and c = 625.6(1) pm] were equal, within calculated standard deviations, for the different batches and in good agreement with previous results (*5–7*).

Details regarding the experimental techniques and the methods for data reduction regarding X-ray diffraction (Enraf–Nonius FR 553, Guinier Simon technique) (*10*), neutron diffraction (collected on the D1B diffractometer at ILL, Grenoble) (*10*), and the intermittently heated adiabatic shield calorimetry (*3*, *11*) have been described earlier.

The heat capacity of the empty calorimeter was determined in a separate series of experiments and represents about 65% of the total. The mass of the sample used in the calorimetric experiments was ~64 g.

Results and Discussion

Structural properties. $Mn_{0.63}Cr_{0.37}As$ crystallizes with the hexagonal NiAs-type structure at high temperatures. Below T_D = 680 K the crystal structure converts to the MnP-type and a continuously increasing orthorhombic distortion develops. The variation in the unit cell dimensions with temperature between 10 and 800 K is shown in Fig. 1. For $T < T_D$ the progressing distortion leads to an increasing $c/(\sqrt{3}b)$ ratio. At T_N = 230 K a magneto-strictive effect due to the onset of long range helimagnetic order (denoted H_c, where c gives

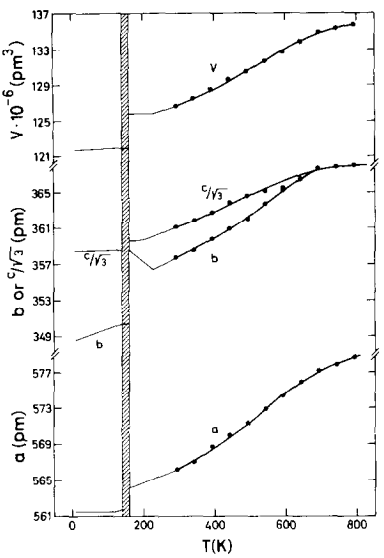

FIG. 1. Temperature dependence of unit cell dimensions for $Mn_{0.63}Cr_{0.37}As$ between 10 and 800 K. Low temperature data represented by thin solid lines are quoted from Ref. (9). Shaded area indicates hysteresis region.

propagation direction of the spirals) provides a significant increase of b with decreasing temperature (see Fig. 1). At T_S = 185 K a first-order, coupled magnetic and structural transition occurs with a large discontinuous change in the unit cell volume. The magnetic structure for $T < T_S$ is also helimagnetic. However, this H_a mode has a quite different arrangement of the spins and the spiral propagation is parallel to the a-axis. All three transitions, at T_D, T_N, and T_S, give rise to large heat capacity effects (see below).

The ordered magnetic moments of the helimagnetic modes are about 1.8 μ_B, whereas the Curie–Weiss law magnetic susceptibility behavior for $T > T_D$ concurs with an effective paramagnetic moment $\mu_p \approx 4.20\ \mu_B$, which, assuming the spin only approximation to be valid, gives a number of unpaired electrons of approximately 3.3. These findings are analogous to the observations for the As-rich samples of $MnAs_{1-x}P_x$. Hence, a continuous spin conversion probably takes place within the temperature domain of the MnP-type phase of $Mn_{0.63}Cr_{0.37}As$. For $MnAs_{1-x}P_x$ this phenomenon gives rise to an extraordinarily large thermal expansivity over a temperature interval of about 300 K, as well as to anomalies in the isothermal compressibility and heat capacity. The thermal expansion coefficient of $Mn_{0.63}Cr_{0.37}As$ goes through a maximum in the region 400–700 K (see Fig. 1). The maximum is, however, much less pronounced than for $MnAs_{0.88}P_{0.12}$. In addition to changes in symmetry and dimensions of the unit cell, the MnP-type distortion causes changes of the atomic arrangement. The metal atoms are displaced mainly parallel to the c-axis and the arsenic atoms mainly parallel to the a-axis (*10*). Powder neutron diffraction data were collected in the temperature interval 295 K $< T < T_D$ in order to determine the degree of the atomic displacements. However, since Mn and Cr have scattering lengths of opposite sign and of approximately equal magnitude, the average scattering contribution from the metal atoms is so small that the metal atom coordinates cannot be refined on the basis of the present data. Therefore, the displacements of the metal atoms were constrained to be equal to those of the As atoms, i.e., $\Delta x_{Mn,Cr} = \Delta x_{As}$ and $\Delta z_{Mn,Cr} = \Delta x_{As}$ (see Ref. (*10*) for comparison of metal and nonmetal displacements). The obtained $\Delta x_{As}(T/T_D)$ relationship is shown in Fig. 2 (Δz_{As} being very much smaller and unimportant in this context). The almost linear variation of Δx_{As} with T/T_D is significantly different from that found for $MnAs_{0.88}P_{0.12}$, indicated in Fig. 2 by the dashed curve. However, this detail does not change the main impact of the transition with respect to the temperature dependence of the interatomic distances.

For $MnAs_{0.88}P_{0.12}$ (*3*) the spin conversion process is assumed to be at its maximum near the temperature where the thermal

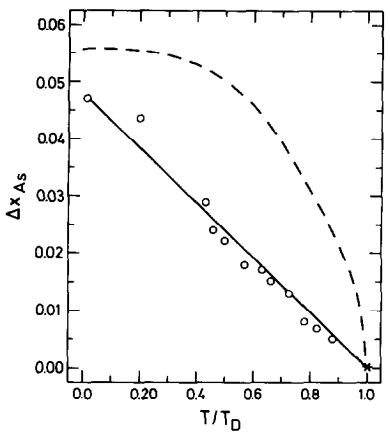

FIG. 2. Variation in distortion parameter $\Delta x_{As} = 1/4 - x_{As}$ with T/T_D. Data for $T/T_D = 0.02$ and 0.21 are taken from Ref. (*7*). Dashed curve represents the same function for $MnAs_{0.88}P_{0.12}$ (*3*).

expansion exhibits its maximum. The overall relative change in unit cell volume, $[V(T_D) - V(10\ K)]/V(T_D)$, is 0.119 for $MnAs_{0.88}P_{0.12}$ (*10*). The corresponding value for $Mn_{0.63}Cr_{0.37}As$ is 0.082, when evaluated using the average volume for the two cooperative magnetic phases, H_a and H_c, both referred to 10 K. For $MnAs_{0.88}P_{0.12}$ the main change in V takes place in a temperature interval of 200 K, where the change in V is $\sim 12 \times 10^{-6}$ pm^3. Over a corresponding temperature interval the volume change of $Mn_{0.63}Cr_{0.37}As$ is much smaller, only $\sim 4 \times 10^{-6}$ pm^3. Similar relationships obtain when comparing the temperature-induced changes of the mean Mn,Cr–As distances. Another important feature of the distortion is that it leads to the occurrence of two additional, relatively short metal–metal distances per metal atom. This process takes place over the entire temperature interval below T_D.

Accordingly, the structural features of $MnAs_{0.88}P_{0.12}$ and $Mn_{0.63}Cr_{0.37}As$ are similar for $T_N < T < T_D$, but with one important distinction: For $MnAs_{0.88}P_{0.12}$ the structural changes and the spin conversion occur in a rather limited temperature range, whereas for $Mn_{0.63}Cr_{0.37}As$ these changes are smeared out over a considerably wider temperature interval.

Heat capacity and thermodynamic properties. The experimental heat capacities of $Mn_{0.63}Cr_{0.37}As$ are given in chronological order in Table I and presented graphically in Fig. 3. In the figure, data also from low temperature measurements (*9*) are included. The peak in the heat capacity curve at ~680 K corresponds to the continuous MnP $\rightleftharpoons$ NiAs-type transition. The two low temperature peaks represent the magnetic order–disorder transition at T_N and the magnetic order–order transition at T_S. In the intermediate temperature interval, $T_N < T < T_D$, the contribution to the heat capacity from the continuous "low" to "high" spin conversion is expected to give rise to another peak. This contribution is, however, only seen as a broad hump in the heat capacity.

The approximate temperature increments used in the determinations can usually be inferred from the adjacent mean temperatures in Table I. The estimated standard deviation of a single heat capacity measurement is about 0.5%. The main reason for the lower accuracy of the present

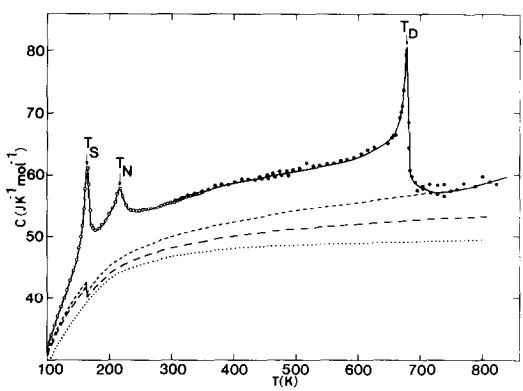

FIG. 3. Heat capacity of $Mn_{0.63}Cr_{0.37}As$. ●, represent results University of Oslo; ○, previous data University of Michigan (*9*). Dashed curves represent estimated nontransitional heat capacity contributions. . . . C_V; ——— $C_V + C_d$, and ——— $C_V + C_d + C_e$.

TABLE II

THERMODYNAMIC PROPERTIES OF $Mn_{0.63}Cr_{0.37}As$ [$M(Mn_{0.63}Cr_{0.37}As)$ = 128.252 G MOLE^{-1}]

T (K)	$C_{p,m}$ (J K^{-1} mole^{-1})	$H^\circ_m(T) - H^\circ_m(0)$ (J mole^{-1})	$S^\circ_m(T) - S^\circ_m(0)$ (J K^{-1} mole^{-1})	$-\{G^\circ_m(T) - H^\circ_m(0)\}/T$ (J K^{-1} mole^{-1})
260	54.28	9204	65.35	29.957
280	54.83	10293	69.39	32.625
298.15	55.47	11299	72.86	34.963
300	55.50	11402	73.20	35.193
325	56.39	12800	77.68	38.295
350	57.30	14221	81.89	41.259
375	58.09	15664	85.87	44.099
400	58.72	17125	89.64	46.828
425	59.21	18599	93.22	49.458
450	59.65	20085	96.62	51.987
475	60.11	21582	99.85	54.414
500	60.65	23091	102.95	56.768
525	61.26	24615	105.92	59.034
550	61.88	26154	108.79	61.237
575	62.45	27709	111.55	63.360
600	63.03	29277	114.22	65.425
625	64.00	30863	116.81	67.429
650	66.30	32488	119.36	69.378
700	57.95	34442	122.21	73.007
725	57.47	35884	124.23	74.735
750	57.44	37319	126.18	76.421
775	57.72	38758	128.06	78.050
800	58.33	40208	129.90	79.640
820	59.07	41382	131.35	80.884

...ued

estimated by use of the low temperature data (*9*) and the Debye model, which assumes harmonic oscillations of atoms around their equilibrium positions. The constant volume heat capacity at low temperatures was estimated from the experimental data (*9*) after subtracting a dilational and an electronic contribution (see below). In the extrapolation to higher temperatures a constant Debye temperature, θ_D = 346 K, was used. It was taken as the maximum value of θ_D when plotted versus temperature.

Additional nontransitional contributions arise from anharmonicity of the lattice vibrations, giving a dilational contribution, and from the excitation of conduction electrons. In the absence of compressibility data it is difficult to evaluate the dilational contribution, $C_d = TV\alpha^2\kappa^{-1}$. As described above, there are large changes in the unit cell dimensions accompanying the continuous MnP $\rightleftharpoons$ NiAs-type transition (see Fig. 1). This enhanced thermal expansion gives rise to a further dilational contribution, in addition to the usual anharmonicity contribution, and should be attributed to the magneto-structural coupling (see below). Under these circumstances the dilational contribution was calculated using the Grüneisen approximation, $C_d = C_V\alpha T\Gamma$. The values of Γ is evaluated at 298.15 K with values for V and C_p taken from Ref. (*9*). The value of the isothermal compressibility is taken as the weighted average of the values for MnAs (*12*) and CrAs (*13*), giving $\kappa = 3.9 \times 10^{-11}$ Pa^{-1}. (Preliminary studies of the compressibility of $Mn_{0.63}Cr_{0.37}As$ using X-ray diffraction indicate a slightly larger value (*14*).) This re-

TABLE I

HEAT CAPACITY OF $Mn_{0.63}Cr_{0.37}As$ [$M(Mn_{0.63}Cr_{0.37}As) = 128.252$ G MOLE^{-1}]

T (K)	$C_{p,m}$ (J K^{-1} mole^{-1})	T (K)	$C_{p,m}$ (J K^{-1} mole^{-1})	T (K)	$C_{p,m}$ (J K^{-1} mole^{-1})	T (K)	$C_{p,m}$ (J K^{-1} mole^{-1})
Series I		338.01	57.02	484.86	60.62	676.73	79.17
647.76	65.93	348.91	57.32	495.63	60.77	680.09	64.20
658.81	67.27	359.64	57.63	506.42	61.02	683.59	60.62
669.70	70.16	370.35	58.23	517.21	61.82	687.11	59.58
680.64	68.43	381.04	58.38	527.92	61.40	690.66	58.70
691.91	58.66	391.65	58.33	538.69	61.40	695.95	57.41
703.47	58.13	402.32	58.81	549.47	61.69	705.05	57.61
715.13	58.45	413.01	59.22	560.28	61.75	716.43	56.99
726.93	58.24	423.73	59.18	571.12	62.21	727.68	56.64
738.81	58.42	434.45	59.13	581.99	62.38	738.73	56.40
		445.19	59.29	592.89	62.73	749.39	57.29
Series II		455.93	59.31	603.80	63.42	759.85	57.55
823.49	59.56	466.67	59.63	614.73	63.97	770.17	58.61[a]
835.53	59.90	477.47	59.92	625.71	64.29	779.74	76.35[b]
847.63	60.12	488.25	59.75			789.42	58.12
859.83	60.22				Series V	799.79	59.62[a]
		Series IV		653.71	66.86	810.66	58.91
Series III		441.60	59.56	656.91	67.19	822.10	58.38
304.77	55.67	452.48	59.96	666.76	69.26		
315.92	56.11	463.35	60.25	670.10	71.08		
327.01	56.63	474.10	60.46	673.43	73.74		

[a] Not used in the final fitting.

[b] Insulation breakdown during energy input.

data [generally the accuracy of the data recorded with the presently used calorimeter is within 0.3% (*11*)] is the small quantity of sample available, which makes the heat capacity of the empty calorimeter dominant.

The experimental heat capacities were fitted to polynomials in temperature by the method of least squares. Values of the thermodynamic functions were obtained from the polynomial expressions by numerical integration using Simpson's rule. The values at the lower temperatures, $T < 350$ K, were obtained on the basis of the present data and the earlier ones by Komada *et al.* (*9*). The agreement between the two sets of data in the region 300 to 350 K is very good. The deviation from the polynomial representation is less than 0.3% for all experimental points. The evaluated thermodynamic data are presented in Table II for selected temperatures. The accuracy in the function values is estimated to be within 0.3%.

The heat capacity of $Mn_{0.63}Cr_{0.37}As$ reported in Ref. (*8*) is lower than the present values by 2.6% at 300 K and by 6.5% at 500 K.

Resolution of the heat capacity. Although the total heat capacity of a sample can be determined with high accuracy, the individual heat capacity contributions from different physical sources are not easily estimated. This problem also concerns the heat capacity contributions from structural and magnetic transitions which are difficult to resolve from the overall values, due to uncertain models for evaluation of the nontransitional contributions. The largest contribution is the constant volume heat capacity, which originates from phonon exitation. This lattice heat capacity can be

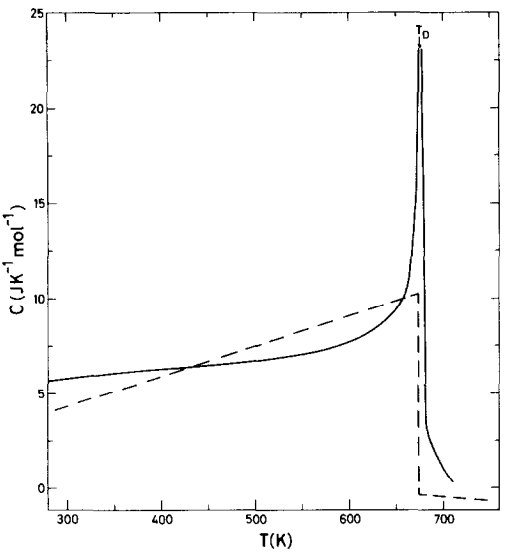

FIG. 4. Excess heat capacity. Dashed curve represents calculated dilational contribution for the strongly coupled magneto-structural transition.

sults in $\Gamma = 1.05$ which is used in the whole temperature range. The thermal expansion coefficient used for evaluating the nontransitional heat capacity at higher temperatures is obtained by using the mean value of α at the low and high temperature sides of the transition region, giving a $\approx 1.0 \times 10^{-4}$ K^{-1} (see Fig. 1).

The electronic contribution, obtained by assuming $C_e = \gamma T$ to be valid even at higher temperatures and by using the value of $\gamma = 19.6$ mJ K^{-2} $mole^{-1}$, evaluated in Ref. (*9*), is unrealistically large. One reason is that the free electron gas heat capacity concept is assumed to be valid also at high temperatures. The resulting high temperature value of the electronic heat capacity will then exceed the value for the classical electron gas, already at 1270 K. Hence, a quite different model is needed at high temperatures, in order that the electronic heat capacity remains a small fraction of the free electron gas value. Another important effect is the neglect of any magnetic heat capacity contributions from the helimagnetic structures at low temperatures (*9*). The presence of any finite magnetic contribution will greatly lower the electronic part. The value of γ used in this study is determined from the difference between C_p and $C_V + C_d$ at high temperatures, which gives $\gamma = 5.89$ mJ K^{-2} $mole^{-1}$.

The evaluated nontransitional heat capacity contributions are given by the dashed curves in Fig. 3, whereas the excess heat capacity is given by the solid curve in Fig. 4. The excess curve is due to the structural MnP $\rightleftharpoons$ NiAs-type transition and the coupled magnetic "low" to "high" spin conversion. The obtained nontransitional curve is somewhat lower than that evaluated by Komada *et al.* (*9*). This is due to the contribution from the spin conversion, which was not considered in the former low temperature study (*9*), where the effect was included as a part of the nontransitional heat capacity.

Coupled crystal structure transition and magnetic spin conversion. Using the phenomenological approach (*2*) which accounts for the anomalous heat capacity of $MnAs_{1-x}P_x$, the main part of the excess heat capacity in Fig. 4 is attributed to the large temperature dependence of the thermal expansion and isothermal compressibility at temperatures below the structural transition. The variation of the unit cell volume and the thermal expansion coefficient are readily obtained from the diffraction data. The thermal expansion coefficient in the relevant temperature range (300–680 K) can be approximated without much error by the constant value $\alpha = 1.5 \times 10^{-4}$ K^{-1}. The values of α at temperatures close to the mangetic order–disorder transition, as well as close to the structural MnP $\rightleftharpoons$ NiAs-type transition, are not easily estimated with good accuracy. As a first approximation discontinuous changes in α at T_N and T_D are assumed. The thermal expansion coefficient for the NiAs-type phase at $T > T_D$, is $\sim 8 \times 10^{-5}$ K^{-1}. The

temperature dependence of the isothermal compressibility is, as for $MnAs_{0.88}P_{0.12}$, not easily obtained. For the phosphorus substituted MnAs, however, the lack of data was overcome by help of the qualitative correspondence between chemical and external pressure (*15*) for low substitutional levels. This method is unfortunately not applicable here, since some of the parameter values are not known. Thus, other ways of evaluating $\kappa(T)$ must be tried. For $MnAs_{0.88}P_{0.12}$, the thermal expansion coefficient and the isothermal compressibility show similar temperature dependence. This may indicate that if a similar relation between κ and α exists also for $Mn_{0.63}Cr_{0.37}As$, the isothermal compressibility will be reasonably well represented by a constant value over the temperature region in question. A crude estimate can, thus, be made using the κ/α ratio observed for $MnAs_{0.88}P_{0.12}$, 1.3 to 2.0 $\times 10^{-7}$ Pa^{-1} K. The chosen value of the isothermal compressibility, 2.25×10^{-11} Pa^{-1}, implies a κ/α ratio of 1.5×10^{-7} Pa^{-1} K in the spin conversion range. The κ-value is lower than that observed for MnAs (*12*) and CrAs (*13*), and is also somewhat lower than suggested by preliminary studies of $Mn_{0.63}Cr_{0.37}As$ (*14*). A somewhat different value will result from a change of the κ/α ratio. From these data, the dilational heart capacity contribution from the magnetically/electronically induced changes in the crystal structure is evaluated (see the dashed curve in Fig. 4). A reasonable agreement between observed and calculated data is obtained, which indicates a strong coupling between the continuously changing paramagnetic moment and the deformation of the high temperature NiAs-type structure. The higher temperature effect, close to T_D, probably originates from large changes in the electronic and atomic frequency distributions, in a direction which gives a significantly lower heat capacity, in the structural transition range.

An approximate value of the enthalpy and entropy increments connected with the combined magnetic spin conversion and the structural transition may be obtained by integrating the excess heat capacity above 260 K, which gives 1730 J $mole^{-1}$ and 4.6 J K^{-1} $mole^{-1}$, respectively. Corresponding values for $MnAs_{0.88}P_{0.12}$ are 4195 J $mole^{-1}$ and 13.31 J K^{-1} $mole^{-1}$. The larger values obtained for the phosphorus substituted MnAs agree with the larger changes in the crystal structure for this phase, which give a larger dilational contribution.

According to Bärner *et al.* (*8*) contributions from a "low" to "high" spin conversion are also observed for CrAs. The curve constructed is, however, not in agreement with the adiabatic calorimetric data reported earlier (*16*). Also for other samples of $Mn_{1-t}Cr_tAs$, "low" to "high" spin effects are reported by Bärner *et al.* (*8*). Their small and very broad maxima are, however, not in accord with the present data. The discrepancy may be ascribed to differences in the preparation of the samples (*5, 7, 17*).

Acknowledgments

This study has been supported by the Norwegian Research Council for Science and the Humanities. We are grateful to Institut Laue Langevin, Grenoble, for the possibility of carrying out the neutron diffraction experiments.

References

1. A. F. Andresen, H. Fjellvåg, O. Steinsvoll, A. Kjekshus, S. Stølen, and K. Bärner, *J. Magn. Magn. Mater.* **62,** 241 (1986).
2. H. Fjellvåg, F. Grønvold, A. Kjekshus, and S. Stølen, *J. Phys. C* **20,** 3005 (1987).
3. A. K. Labban, E. F. Westrum, Jr., H. Fjellvåg, F. Grønvold, A. Kjekshus, and S. Stølen, *J. Solid State Chem.* **70,** 185 (1987).
4. K. Katoh and K. Motizuki, *J. Phys. Soc. Japan* **53,** 3166 (1984).
5. R. Wöhl, H. Berg, and K. Bärner, *Phys. Status Solidi A* **57,** 179 (1980).

6. S. Haneda, N. Kazama, Y. Yamaguchi, and H. Watanabe, *J. Phys. Soc. Japan* **42,** 1212 (1977).
7. H. Fjellvåg and A. Kjekshus, *Acta Chem. Scand. A* **38,** 1 (1984).
8. K. Bärner, C. Santandrea, U. Neitzel, and E. Gmelin, *Phys. Status Solidi B* **123,** 541 (1982).
9. N. Komada, E. F. Westrum, Jr., H. Fjellvåg, and A. Kjekshus, *J. Magn. Magn. Mater.* **65,** 37 (1987).
10. H. Fjellvåg, A. Kjekshus, and S. Stølen, *J. Solid State Chem.* **64,** 123 (1986).
11. F. Grønvold, *Acta Chem. Scand.* **21,** 1695 (1967).
12. N. P. Grazhdankina and Y. S. Bersenev, *Zh. Eksp. Teor. Fiz.* **50,** 1519 (1966) (transl. *Sov. Phys. JETP* **23,** 1013 (1966)).
13. V. I. Kamenev and E. A. Zavadskii, *Fiz. Tverd. Tela (Leningrad)* **20,** 933 (1978) (transl. *Sov. Phys. Solid State* **20,** 541 (1978)).
14. U. Sondermann, personal communication.
15. A. Zieba, R. Zach, H. Fjellvåg, and A. Kjekshus, *J. Phys. Chem. Solids* **48,** 79 (1987).
16. R. Blachnik, G. Kudermann, F. Grønvold, A. Alles, B. Falk, and E. F. Westrum, Jr., *J. Chem. Thermodyn.* **10,** 507 (1978).
17. A. F. Andresen, K. Bärner, H. Fjellvåg, K. Heinemann, A. Kjekshus, and U. Sondermann, *J. Magn. Magn. Mater.* **58,** 287 (1986).